Synthetic Metals 257 (2019) 116182

Contents lists available at ScienceDirect

Synthetic Metals

journal homepage: www.elsevier.com/locate/synmet

1 V high open-circuit voltage fluorinated alkoxybiphenyl side-chained benzodithiophene based photovoltaic polymers

Wen Cui[a], Feng Li[b], TingTing Zhu[a], Yonghai Li[c], Liangmin Yu[d], Renqiang Yang[c], Mingliang Sun[a,*]

[a] School of Materials Science and Engineering, Ocean University of China, Qingdao, 266100, China
[b] Key Laboratory of Rubber-Plastics of Ministry of Education/Shandong Province, School of Polymer Science and Engineering, Qingdao University of Science & Technology, Qingdao, 266042, China
[c] CAS Key Laboratory of Bio-based Materials, Qingdao Institute of Bioenergy and Bioprocess Technology, Chinese Academy of Sciences, Qingdao, 266101, China
[d] Key Laboratory of Marine Chemistry Theory and Technology, Ministry of Education, Ocean University of China, Qingdao, 266100, China

ARTICLE INFO

Keywords:
Conjugated polymers
Polymer solar cells
Benzodithiophene (BDT)
Fluorinated alkoxybiphenyl side-chain
High open-circuit voltage

ABSTRACT

Utilizing two-dimensional (2-D) conjugated structure and extending two-dimensional π-conjugation system with benzene can improve the performance of the BDT-based polymer solar cells (PSCs). In this work, combining with strong electron-drawing ability of fluorine atom, a new monomer BBFBDT with fluorinated alkoxybiphenyl unit as side-chain was designed and synthesized to construct medium band-gap donor (D) - acceptor (A) copolymer P1 with a benzo[1,2- c:4,5-c']dithiophene-4,8-dione (BDD) acceptor. Blending with a classical non-fullerene acceptor ITIC, the P1-based PSCs reached a power conversion efficiency (PCE) of 4.16% and when coupled with a fullerene acceptor $PC_{71}BM$, the PCE of PSCs reached 4.66% with an open-circuit voltage (V_{oc}) of 0.93 V, a short-circuit current density (J_{sc}) of 9.83 mA cm^{-2} and a fill factor (FF) of 50.97%. The relatively poor J_{sc} of P1-based devices may be caused by the bad complementarity of absorption spectra. Furthermore, a wide band-gap D-A copolymer P2, with a electron-deficient 4,7-bis(5-bromothiophen-2-yl)-2-((2-ethylhexyl)oxy)-5,6-difluoro-2H-benzo[d][1,2,3]triazole (TZ) as the acceptor unit, was synthesized to match the absorption spectra of ITIC. Finally, the efficiency achieved 6.59% with V_{oc} of 0.99 V, J_{sc} of 14.37 mA cm^{-2} and FF of 46.32%.

1. Introduction

Bulk heterojunction polymer solar cells (BHJ-PSCs) have been considered to be promising flexible light harvesting devices for clean and renewable energy conversion due to the advantages of light weight, large area and low cost [1–9]. As for photoactive layers, the blending of conjugated polymer donor and small molecular acceptor has been proven to be efficient structures for single junction PSCs devices [10]. The classical fullerene acceptor, such as [6, 6]-phenyl-(C_{61} or C_{71})-butyric acid methyl ester ($PC_{61}BM$ or $PC_{71}BM$), have been widely used in the construction of D-A structure [11–13] and the power conversion efficiency (PCE) of PSCs, comprising of polymer donor and fullerene acceptor, have achieved exceed 10% [14]. Recently, a novel non-fullerene acceptor ITIC was reported by Zhan's group [15] which attracted wide interest for the easily tunable energy levels and more complementary absorption relative to fullerene acceptor [16–19]. Up to now, the PCE of non-fullerene PSCs surpassed 14% due to the tremendous progress of modifying donor and acceptor structures and improving the device processing techniques, which promoted the development of high-performance polymer solar cells [20,21].

In order to achieve high value of short-circuit current (J_{sc}), open-circuit voltage (V_{oc}) and fill factor (FF) of PSCs, one of the most efficient strategies is modifying structure of conjugated polymer donor to bring out suitable energy levels and complementary absorption matched with acceptor. In recent years, benzodithiophene (BDT)-based conjugated polymers donor have become the focus of studying and achieved remarkable results [7,22–25]. Many works have reported that introducing conjugated side chains and electron-withdrawing substituents to BDT backbone were effective approaches to intensify charge transport in D–A conjugated polymers and improve photovoltaic properties of organic solar cells [20,25–30]. Among them, fluorination has been proven to be an efficient strategy to alter the morphology of the photoactive layer through the interactions of weak bonds (such as CFe···H and F···S) and manipulate the energy level of polymer donor due to the strong electron-withdrawing ability, thereby get higher V_{oc} value [31–34]. Yang's group have reported that introducing *o*-fluoro-*p*-alkoxyphenyl group to BDT unit was effective to improve the performance of PSCs [35]. Moreover, it has been proven that extending two-

* Corresponding author.
E-mail address: mlsun@ouc.edu.cn (M. Sun).

https://doi.org/10.1016/j.synthmet.2019.116182
Received 24 June 2019; Received in revised form 17 August 2019; Accepted 19 September 2019
Available online 12 October 2019
0379-6779/

dimensional π-conjugation length of side chains can also improve the device performance [27,36]. For example, Wang's group reported that polymer PBDTBzT–DTffBT, with two-dimensional π-extended side-chain (benzothienyl), exhibited improved PCE compared with polymer PBDTT-DTffBT, which based on thienyl-substituted BDT [37]. However, the influence to the performance of PSCs about combining the fluorine substitution and π-extended side chains on the BDT backbone was not reported so far. Fluorination 2D π-conjugation side chains can take the advantage of both fluorination and 2D π-conjugation, which maybe further improve the photovoltaic properties of PSCs. Based on the above considerations, we designed and synthesized a new electron-rich building block, fluorinated-alkoxybiphenyl-substituted BDT unit, to construct medium band-gap copolymers P1 with BDD acceptor unit. Blending with $PC_{71}BM$, the maximum PCE of P1-based device was 4.66% with V_{oc} = 0.93 V, J_{sc} =9.83 mA cm^2 and FF = 50.91% after thermal annealing. While blending with ITIC, the P1-based PSCs reached a relatively poor efficiency of 4.16%. Unfortunately, although high V_{oc} value yielded, J_{sc} value was low as the result of mismatched absorption with acceptor. In order to adjust the complementarity of absorption spectra, a new wide-gap D-A copolymer P2 was synthesized with BBFBDT and TZ through the Stille coupling reaction. Finally, the maximum PCE of P2 achieved 6.59% with V_{oc} of 0.99 V, J_{sc} of 14.37 mA cm^{-2} and FF of 46.32%. The chemical structures of polymer donors and small molecular acceptors and configuration of BHJ-PSCs are given in Fig. 1. This work investigated the influence of novel polymer structure on optical properties, electrochemical properties, photovoltaic properties, molecular conformations and BHJ blend film morphology and provides experiences to design new photovoltaic polymers in the future.

2. Materials and methods

2.1. Synthesis ofmaterials

In this work, starting chemicals and solvent used for the experiment were purchased from commercial companies without other further purification. The reagents used for water-sensitive reactions, such as tetrahydrofuran (THF) and toluene, were distilled by sodium under an argon atmosphere. According to reported literatures, compounds TZ-Br and BDD-Br were synthesized. The synthetic routes of polymers P1, P2 are given in Scheme 1 and the detailed description is shown below.

Synthesis of Bromo-3-fluoro-4′-((2-hexyldecyl)oxy)-1,1′-biphenyl (3): 1-bromo-4-((2-hexyldecyl)oxy)benzene (1) was synthesized according to reported literature [35]. A dried 300 ml four-neck flask was charged with 1-bromo-4-((2-hexyldecyl)oxy)benzene (1) (3.0 ml, 24 mmol) in dry THF (170 ml) solvent under argon gas atmosphere. Then n-Butyllithium (n-BuLi, 15 mL, 24 mmol, 1.6 mol L^{-1}) was added to the mixture dropwise under -78 °C and stirred at this temperature for 2 h. Next, 2-isopropoxy- 4,4,5,5-tetramethyl-1,3,2-dioxaborolane (9.5 mL) was added in the mixture. After keeping the reaction at -78 °C for another two hours, the mixture was stirred at room temperature overnight. The mixture was neutralized with 1 N HCl to pH = 7 and extracted with ethyl acetate. Then the solution was washed using brine and dried with anhydrous $MgSO_4$. After the solvent was evaporated, the crude product was purified with silica-gel column chromatography by using ethyl acetate as eluent to afford 2-(4-((2-hexyldecyl)oxy)phenyl)-4,4,5,5-tetramethyl-1,3,2-dioxaborolane (2) (5.6 g, 99%) as colorless liquid. A 300 ml four-neck flask was charged with 2-(4-((2-hexyldecyl) oxy)phenyl)-4,4,5,5-tetramethyl-1,3,2-dioxaborolane (2) (5.0 g, 21 mmol), 1-bromo-2-fluoro-4-iodobenzene (1.8 mL, 20 mmol), PPh_3 (2.6 g, 9.8 mmol), 2 M K_3PO_4 (50 mL) and 1,4-dioxane (130 mL). The oxygen in the flask was removed by N_2 bubbling degassing. Then Pd $(PPh_3)_4$ (1.4 g, 1.2 mmol) was added to the solution and the mixture was stirred at 100 °C for overnight. Then water was added to the mixture and the mixture was extracted with AcOEt. The organic layer was dried with anhydrous $MgSO_4$. After the solvent was evaporated, the crude product was purified with silica-gel column chromatography using hexane as eluent to afford 4-bromo-3-fluoro-4′-((2-hexyldecyl) oxy)-1,1′-biphenyl (3) (3.1 g, 77%) as light yellow solid.

^{1}H NMR (600 MHz, $CDCl_3$) δ 7.59 – 7.52 (m, 1 H), 7.47 (d, J =8.7 Hz, 2 H), 7.30 (dd, J = 10.0, 2.0 Hz, 1 H), 7.21 (dd, J = 8.3, 2.0 Hz, 1 H), 6.97 (d, J =8.7 Hz, 2 H), 3.87 (d, J =5.7 Hz, 2 H), 1.80 (dt, J = 12.2, 6.0 Hz, 1 H), 1.43 – 1.24 (m, 24 H), 0.89 (m, J = 6.7, 3.7 Hz, 6 H).

Synthesis of 4,8-bis(3-fluoro-4′-((2-hexyldecyl)oxy)-[1,1′-biphenyl]-4-yl)benzo[1,2-b:4,5-b']dithiophene (BBFBDT): In a 100 ml round-bottom flask, the compound 4-bromo-3-fluoro-4′-((2-hexyldecyl)oxy)-1,1′-biphenyl (3) (6.31 g, 13.02 mmol) was dissolved in THF (50 mL) and cooled to -78 °C under argon atmosphere. N-Butyllithium (9.06 mL, 14.51 mmol, 1.6 mol L^{-1}) was dropped slowly into the solution. After keeping the mixture at -78 °C for two hours, benzo[1,2-b:4,5-b']

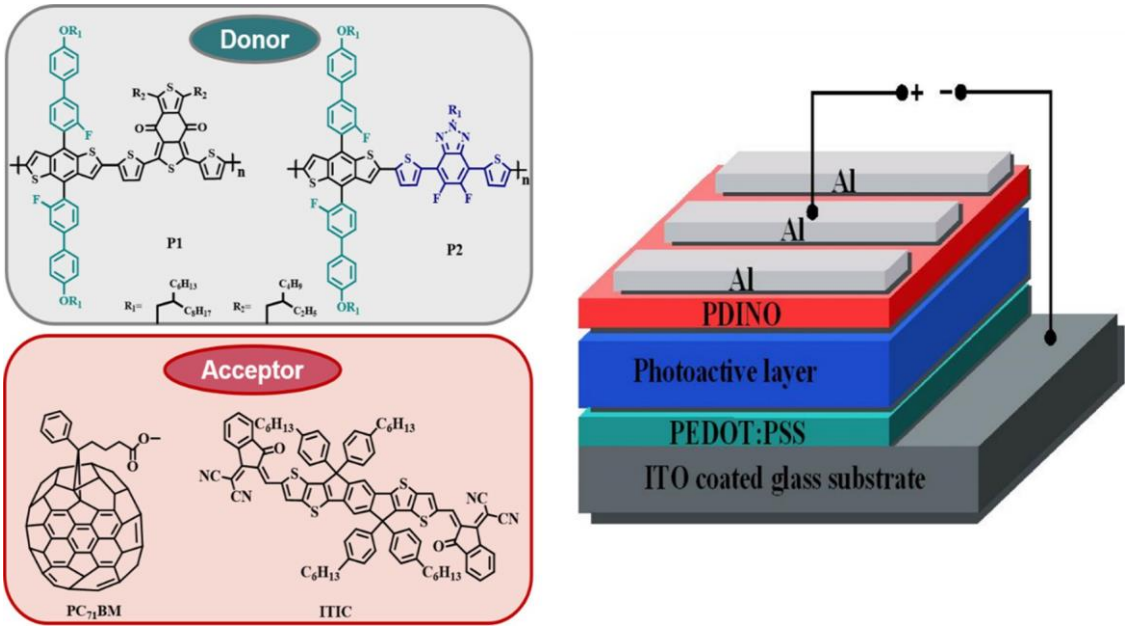

Fig. 1. Chemical structure of polymer donors and small molecular acceptors and configuration of BHJ-PSCs.

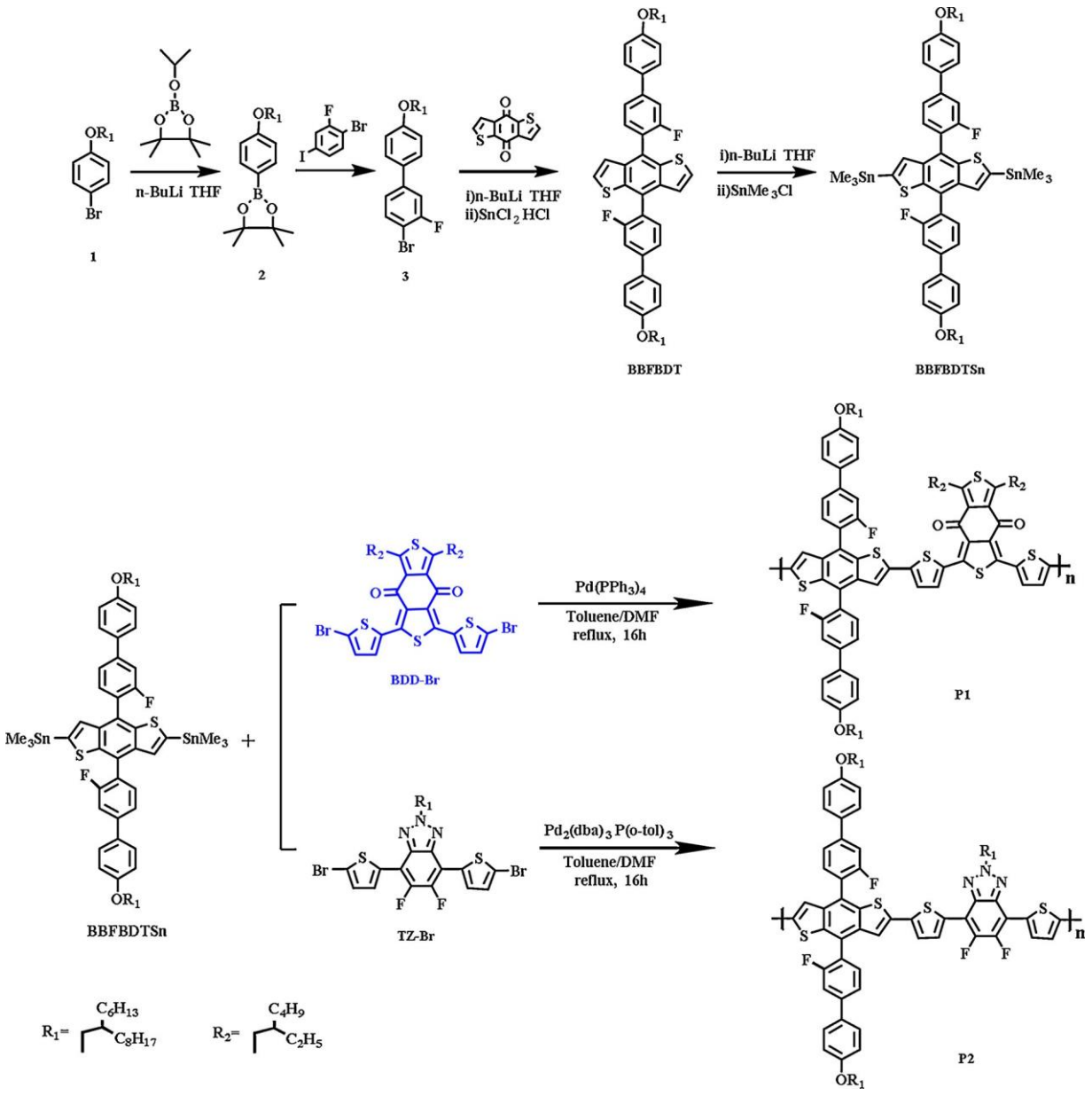

Scheme 1. Synthetic routes and chemical structures of monomer and polymers.

dithiophene-4,8-dione (1.03 g, 4.56 mmol) was poured into the flask. The mixture was heated to room temperature and stirred overnight. $SnCl_2{\cdot}2H_2O$ dissolved in 10% HCl (20 mL) was bubbled by argon for three hours and then injected to the flask. After the solution stirring for four hours at 70 °C, 20 ml water was added into the reaction. The mixture was extracted by diethyl ether and a white solid (BBFBDT) was obtained (1.6 g, 48% yield) after being purified further by column chromatography using dichloromethane and petroleum ether.

^{1}H NMR (600 MHz, $CDCl_3$) δ 7.71 (dt, J = 12.9, 7.7 Hz, 1 H), 7.64 (d, J = 8.6 Hz, 2 H), 7.57 – 7.53 (m, 1 H), 7.51 (d, J = 10.9 Hz, 1 H), 7.47 – 7.44 (m, 1 H), 7.26 – 7.22 (m, 1 H), 7.04 (d, J = 8.7 Hz, 2 H), 3.92 (d, J = 5.7 Hz, 2 H), 1.83 (dt, J = 12.1, 6.0 Hz, 1 H), 1.41 – 1.24 (m, 24 H), 0.90 (q, J = 6.8 Hz, 6 H). ^{13}C NMR (151 MHz, $CDCl_3$) δ 160.86, 143.52, 138.52, 136.70, 136.69, 131.93, 131.60, 128.10, 127.46, 127.44, 124.64, 115.04, 77.22, 38.01, 31.93, 31.42, 30.05, 29.72, 29.62, 29.61, 29.36, 29.35, 26.88, 22.69, 14.14.

Synthesis of (4,8-bis(3-fluoro-4′-((2-hexyldecyl)oxy)-[1,1′-biphenyl]-4-yl)benzo[1,2-b:4,5-b']dithiophene-2,6-diyl)bis(trimethylstannane) (BBFBDTSn): BBFBDT (1.49 g, 1.52 mmol) was dissolved in dry THF (30 mL) under an argon atmosphere and n-BuLi (2.53 mL, 4.06 mmol, 1.5 mol L^{-1}) was dropped slowly into the solution at 0 °C. After keeping the mixture at 0 °C for two hours, trimethyltin chloride (5.23 mL, 5.25 mmol, 1.3 mol L^{-1}) was injected into the flask. The mixture was stirred at room temperature overnight and stopped with water. Diethyl ether was poured to extract the raw product, and then the solvent was removed. Then raw product was purified by recrystallization from acetone, and a white solid (BBFBDTSn) was obtained (1.23 g, 61% yield). MALDI-TOF (*m/z*): calcd for BBFBDTSn, 1337.13; found 1336.256 (M^+).

^{1}H NMR (600 MHz, $CDCl_3$) δ 7.74 – 7.69 (m, 1 H), 7.66 (d, J = 8.6 Hz, 2 H), 7.57 – 7.50 (m, 2 H), 7.24 (m, J = 12.4 Hz, 1 H), 7.04 (d, J = 8.6 Hz, 2 H), 3.92 (d, J = 5.6 Hz, 2 H), 1.83 (dt, J = 12.0, 5.8 Hz, 1 H), 1.41 – 1.26 (m, 24 H), 0.90 (q, J = 6.6 Hz, 6 H), 0.43 – 0.31 (m, 9 H). ^{13}C NMR (151 MHz, $CDCl_3$) δ 167.73, 154.70, 153.54, 147.10, 141.00, 139.54, 137.05, 130.89, 128.56, 126.20, 125.66, 124.90, 118.11, 116.95, 116.33, 114.82, 114.49, 71.93, 39.55, 39.48, 30.53, 30.50, 29.15, 29.12, 23.88, 23.11, 14.15.

Synthesis of polymer P1 and P2: BBFBDTSn (133.71 mg, 0.1 mmol),

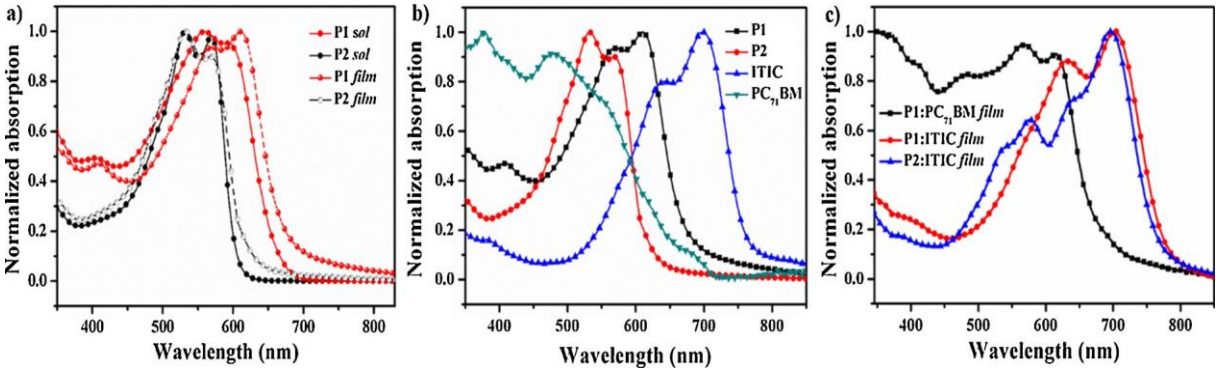

Fig. 2. (a) UV–vis absorption spectra of P1 and P2 in CB diluted solutions and as the thin films; (b) The film absorption spectra of the P1, P2, $PC_{71}BM$ and ITIC; (c) The absorption spectra of the P1: $PC_{71}BM$, P1: ITIC and P2:ITIC blend films (1:1.5, w/w).

BDD-Br (76.67 mg, 0.1 mmol) or TZ-Br (71.86 mg, 0.1 mmol), Pd $(PPh_3)_4$ (7.12 mg, 0.1 mmol) or $Pd_2(dba)_3$ (1.37 mg, 0.1 mmol), P(*o*-tol)$_3$ (2.74 mg, 0.1 mmol) were added to a dry flask. After the addition of dry toluene (8 mL) and dry dimethylformamide (DMF, 0.6 mL), the mixture was reacted for 16 h. After being cooled down to room temperature, the mixture was poured into methanol. The precipitate was collected and subjected to soxhlet extraction with methanol, acetone and hexane as the solvents to remove small molecules and oligomers. The product was then purified by silica gel column chromatography using CB as an eluent. After the solvent was removed, the resulting purple film was obtained with the addition of 30 ml methanol and then dried under vacuum for 24 h at 40 °C.

2.2. Materials characterization methods

The molecular weight (M_n) and polydispersity index (PDI) were estimated by gel permeation (GPC) analysis on an ELEOS system using THF as the eluent. Thermogravimetric analysis (TGA) of polymers were performed via a STA-449 instrument in a nitrogen atmosphere. The UV–vis spectra were obtained using Hitachi U-4100 spectrophotometer under room temperature. The electrochemical cyclic voltammetry (CV) curves were recorded using CHI 660D electrochemical workstation with a polymer coated glassy carbon as working electrode, a platinum wire as counter electrode and a saturated calomel reference electrode (SCE). In this system, the electrolyte is prepared from the acetonitrile solution and 0.1 M tetrabutylammonium hexafluorophosphate (Bu_4NPF_6). The transmission electron microscopy (TEM) measurement was obtained via a HITACHI H-7650 electron microscope working at an acceleration voltage of 100 kV.

2.3. Device fabrication and evaluations

The photovoltaic devices with a classical structure of ITO/PEDOT: PSS/active layer/PDINO/Al were prepared in the nitrogen atmosphere. The ITO coated glass substrates (15 mm x 15 mm) were cleaned in an ultrasonic bath for 15 min with the following solvent: ITO detergent, ultrapure water, acetone and isopropanol. After dried by nitrogen and cleaned by oxygen plasma for 3 min, the ITO-coated substrates were spin-coated with PEDOT:PSS hole transport layer at 4000 rpm for 30 s, following annealing at 150℃ for 15 min in air. Polymer P1and $PC_{71}BM$ were dissolved in o-dichlorobenzene (o-DCB) at the concentration of 28 mg ml^{-1} with weight ratios of 1:1, 1:1.5 and 1:2. Polymer P2 and ITIC were dissolved in chlorobenzene (CB) at the concentration of 16 mg ml^{-1} with weight ratios of 1:1, 1:1.5 and 1:2. Then the blend solution were spin-coated onto PEDOT: PSS substrates as the photoactive layer in the glovebox. Next, a 10 nm thickness PDINO electron transport layer were spin-coated onto the top of the active layer at 3000 rpm for 25 s carefully. Finally, to form the top electrode of the devices, a 100 nm thickness Al was deposited thermally onto the former film in a vacuum evaporator. The devices based on P1:$PC_{71}BM$ and P2: ITIC were characterized under AM 1.5 G radiation, with the intensity of 100 mW cm^{-2}.

3. Results and discussion

3.1. Synthesis and characterization

The synthetic routes and chemical structures of the new monomer BBFBDT and polymers P1 and P2 are outlined in Scheme 1, and the detailed synthetic process and conditions are provided in the experimental section. The intermediate product, new monomer BBFBDT and polymers in the synthesis procedures were characterized by ^{1}H NMR and ^{13}C NMR (Figs. S1–S5). The BDD-Br and TZ-Br compounds were synthesized according to the previously reported methods [38–41]. The polymers P1 and P2 were prepared via Stille coupling reaction in anhydrous toluene with different catalyst. Both polymers exhibit acceptable solubility in chlorobenzene (CB) and *o*-dichlorobenzene (o-DCB) at room temperature. Estimated by gel permeation chromatography (GPC) with polystyrene as the standard and tetrahydrofuran (THF, 40 °C) as the eluent, the number-average molecular weights (M_n) and polydispersity index (PDI = M_w / M_n) of polymers P1 and P2 are 21.6 kDa/1.40 and 20.5 kDa/1.21, respectively. The thermal properties of the polymers were evaluated by thermogravimetric analysis (TGA) with a heating rate of 10 °C min^{-1} in a nitrogen atmosphere (Fig. S6). The onset decomposition temperatures (T_d) with a 5% weight loss of P1 and P2 are calculated to be 400 °C and 340 °C, respectively. This result indicates that the polymers possess good thermal stability, which is helpful to the further characterization and the fabrication of PSCs devices [43].

3.2. Optical and electrochemical properties

The normalized ultraviolet-visible (UV–vis) of the polymers in dilute chlorobenzene (CB) solutions and as thin films are both shown in Fig. 2a, and relevant data are collected in Table 1. In dilute CB solution, the strong absorption peaks of polymers P1 and P2 are located at about 620 nm and 530 nm, respectively, which corresponding to the intramolecular charge transfer (ICT) in the donor-acceptor system [42]. In addition, polymer P1 shows the weak absorption band at 410 nm due to the π-π* transitions [36]. Whether in solution or as films, both polymers display sharp shoulder peaks [43]. These two polymers have good planarity, the interaction between the polymers backbones cause strong molecular aggregation, which explains the sharp shoulder peaks observed in the UV-absorption spectra, and it's also consistent with the works reported in the past [31,35]. Furthermore, the UV–vis absorption spectra of the polymers in film state exhibit slight red shift compared to that in solution, as a result of the increased inter- and intra-molecular interactions [44]. Compared to the solution state, the interaction

Table 1
Decomposition temperatures, molecular weights, UV–vis absorption properties and molecular energy levels of polymers.

Polymer	T_d(°C)	M_n(kDa)	λ_{max}film (nm)	λ_{max}solution (nm)	λ_{onset}film (nm)	E_g^{opt}(eV)	E_{ox} (V)	HOMO* (eV)	LUMO* (eV)
P1	400	21.6	620	560	670	1.85	1.05	−5.37	−3.52
P2	340	20.5	530	530	625	1.98	1.21	−5.34	−3.36

*Molecular energy levels are calculated from cyclic voltammograms.

between the backbones of these two polymers in the film state is stronger with more ordered stacking, and thus the inter-molecular distances become smaller, which are beneficial to enhance the π-π stacking between the polymer backbones and reduce the energy required for π electronic transitions, and thereby caused slight red shift [37]. Moreover, the temperature-dependent UV–vis absorption spectra of the polymers (from 20 °C to 90 °C) were further measured to evaluate intermolecular interactions. As shown in Fig. S7, the shoulder peaks of polymers P1 and P2 decrease gradually with the rise of temperature but still exist in hot solvents (CB, 60 °C and 90 °C), which indicate that polymers possess strong intermolecular interactions. In addition, the optical band-gaps of the polymers P1 and P2 were calculated to be 1.85 eV and 1.98 eV, respectively, according to the equation $E_g^{opt} = 1240/\lambda_{onset}$ (λ_{onset} is the onset of the absorption spectra of the thin film). In order to achieve complementary and broad absorption range, polymers P1 and P2 probably require different acceptor materials. As shown in Fig. 2b, we can see that the absorption spectra of P1 and P2 matched well with that of $PC_{71}BM$ and ITIC, respectively. The absorption spectra of the P1:$PC_{71}BM$, P1: ITIC and P2: ITIC blend films (1:1.5, w/w) are displayed in Fig. 2c. In the visible range, the absorption range of P2: ITIC blend film is distinctly expanded than that of P1:$PC_{71}BM$ and P1: ITIC blends, which is beneficial for harvesting more solar photons and enhancing value of J_{sc}.

The oxidation/reduction potentials of polymers can be measured utilizing electrochemical cyclic voltammetry (CV). As shown in Fig. 3a and Table 1, the onset oxidation potential (E_{ox}) of the polymers P1 and P2 are 1.05 V and 1.21 V, respectively. The highest occupied molecular orbital (HOMO) and the lowest unoccupied molecular orbital (LUMO) energy levels of polymers P1 and P2, estimating by the following equations: $E_{HOMO} = -e (E_{ox} + 4.8 - \phi_{1/2}, FeCp_2)$ (eV); $E_{LUMO} = E_{HOMO} + E_g^{opt}$ (eV), are -5.37 eV, -3.52 eV and -5.34 eV, -3.36 eV, respectively. The redox potential of the Fc/Fc^+ internal reference was 0.39 V. From Fig. 3b, we can see both polymers display deep HOMO energy levels, which are beneficial to achieve high V_{oc} [27].

3.3. Theoretical calculations

To further explore the influence of introducing the novel conjugated side chain to the molecular conformations and electronic properties of polymers, theoretical calculation was performed employing density functional theory (DFT) at the B3LYP/6-31G* level. All long alkyls were replaced by methyl and just choose two repeating units as the object of calculation in order to simplify calculations. As shown in Fig. 4, the dihedral angles between the side chain and BDT backbone of P1 and P2 are 60.88° and 60.72°, respectively. And the dihedral angles between benzene and fluorobenzene unit in side chain are close to 37°. This highly twisted side groups help to obtain good solubility of polymers and deep HOMO energy levels [45]. By contrast, the dihedral angles between the polymer backbones are small (< 21°), which form relatively planar backbone conformations and thereby benefit the charge transport along the polymer backbones [46]. The energy levels obtained by DFT are also given in Fig. 4, which coincide well with the experimental results from cyclic voltammetry. The HOMO energy levels of both polymers are distributed equally over both donor and acceptor units, while the LUMO energy levels are mainly localized on acceptor units. V_{oc} is related to the energy difference between the HOMO levels of the donor material and the LUMO levels of the acceptor material [22]. In the computational (theoretical) and cyclic voltammetry analysis, both polymers show similarly low HOMO energy levels, which are helpful to obtain high V_{oc} values.

3.4. Photovoltaic properties and analysis

In order to study the photovoltaic characteristics of the synthesized polymers more meticulous, BHJ polymer solar cells were made with a configuration of ITO/PEDOT: PSS/active layer /PDINO/Al. The detail data to optimize the performance of the devices under AM 1.5 G radiation (100 mW cm^{-2}), such as the weight ratios of donor: acceptor in the blend films and the processing conditions, are summarized in Table S1 and the corresponding current density-voltage (*J-V*) curves of the devices are shown in Fig. S8. From Table 2, we can see that the PCE of PSCs based on P1:$PC_{71}BM$ achieve 4.33% with V_{oc} = 0.91 V, J_{sc} =9.91 mA cm^{-2} and FF = 48.01% without thermal annealing under the optimal D: A blend ratio (w/w = 1:1.5). In addition, the PSCs based on P1: ITIC was also characterized, although the values of V_{oc} and J_{sc} were enhanced, the film-forming property dropped so that the PCE was

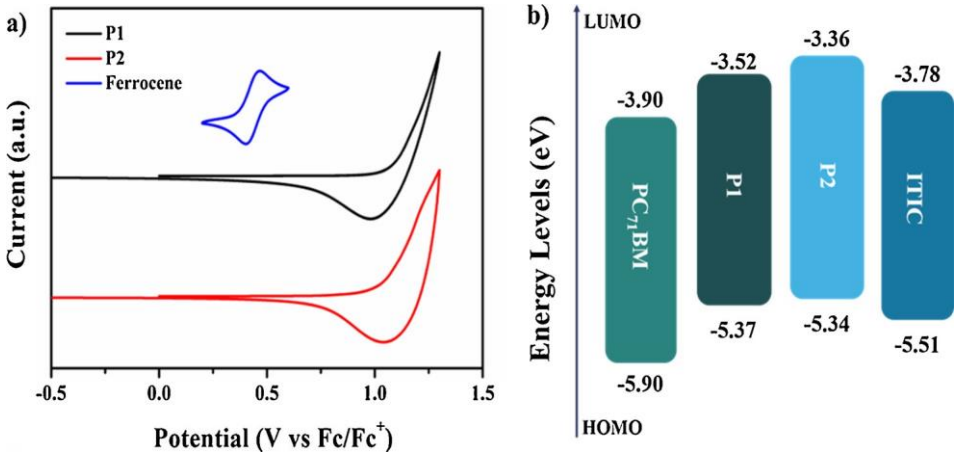

Fig. 3. (a) Cyclic voltammograms of P1, P2 and ferrocene; (b) Energy diagram of $PC_{71}BM$, P1, P2 and ITIC.

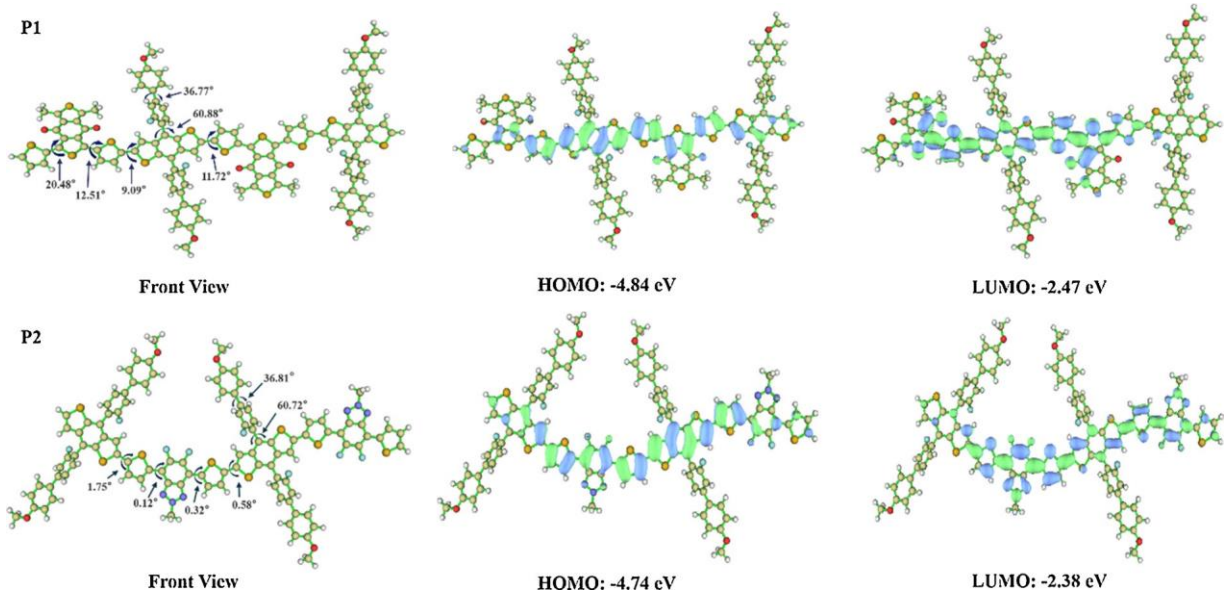

Fig. 4. Optimized molecular conformations, dihedral angles and frontier molecular orbitals for P1 and P2 obtained by DFT calculations.

Table 2
The photovoltaic parameters of the devices with P1:ITIC, P1:$PC_{71}BM$ and P2:ITIC under different conditions.

Blend	Annealing	V_{oc} (V)	J_{sc} (mA cm^{-2})	FF (%)	PCE_{max}
P1:ITIC	no	0.98	9.78	39.02	3.74
P1:ITIC	120 °C	0.97	10.21	42.00	4.16
P1:$PC_{71}BM$	no	0.91	9.91	48.01	4.33
P1:$PC_{71}BM$	120 °C	0.93	9.83	50.97	4.66
P2:ITIC	no	0.99	13.72	43.51	5.91
P2:ITIC	90 °C	0.99	14.37	46.32	6.59

not high than that of PCSs based on P1:$PC_{71}BM$. As shown in Fig. 2b, the UV–vis absorption spectra of P1 are heavily overlapped with that of $PC_{71}BM$ and ITIC, which is not good for harvesting solar light, so the J_{sc} values are relatively poor whether P1 blends with $PC_{71}BM$ or ITIC. The PCE of the P2-based PSCs coupled with non-fullerene acceptor ITIC (w/w = 1:1.5) is 5.91% with V_{oc} = 0.99 V, J_{sc} =13.72 mA cm^{-2} and FF = 43.51% without thermal annealing. The broader absorption range of P2: ITIC blend film compared to that of P1:$PC_{71}BM$ and P1: ITIC blend films, shown in Fig. 2c, may be the reason for the increased J_{sc} of P2-based PSCs. It is noticeable that the PCE of P1-based PSCs up to 4.66% with V_{oc} = 0.93 V, J_{sc} =9.83 mA cm^{-2} and FF = 50.97% after 120 °C annealing and the devices based on P2 exhibit the enhanced PCE of 6.59% with V_{oc} = 0.99 V, J_{sc} =14.37 mA cm^{-2} and FF = 46.32% after 90 °C annealing. The annealing improved devices performances may be attributed to the improved active layer morphology (Fig S9). The *J–V* curves of the polymer solar cells based on synthesized polymers under optimal conditions are given in Fig. 5a.

The external quantum efficiency (EQE) curves of the devices based on P1:$PC_{71}BM$ and P2: ITIC under corresponding optimal conditions were measured to further investigate photocurrent response of the above PSCs. The current density calculated by EQE curves, 9.74 mA cm^{-2} for P1 and 14.24 mA cm^{-2} for P2, were basically consistent with J_{sc} measured by *J–V* curves. As shown in Fig. 5b, the devices prepared with P1 and P2 exhibit strong and broad photocurrent response in the range of 350–700 nm and 400–800 nm, respectively. Contrast to the photocurrent response of P1-based PSCs, the maximum EQE values of P2-based device achieves 65% and remain stable from 550 to 750 nm, which contributing to higher J_{sc} of P2-based PSCs [47]. The photoluminescence (PL) emission spectra of pure polymers P1, P2 and P1:$PC_{71}BM$, P2: ITIC blended films are exhibited in Fig. S10. The PL emissions of pure polymers are largely quenched when blending with acceptor materials, which indicates that the efficient photo-induced exciton separation and charge transfer between the donor and acceptor materials [17].

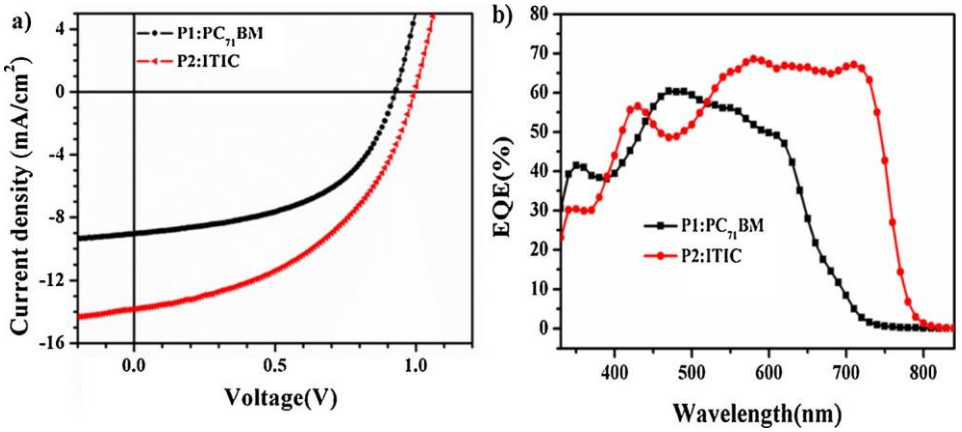

Fig. 5. (a) *J–V* curves of the optimized solar cells based on polymers P1 and P2 under AM1.5 G radiation (100 mW cm^{-2}); (b) EQE curves of the corresponding devices.

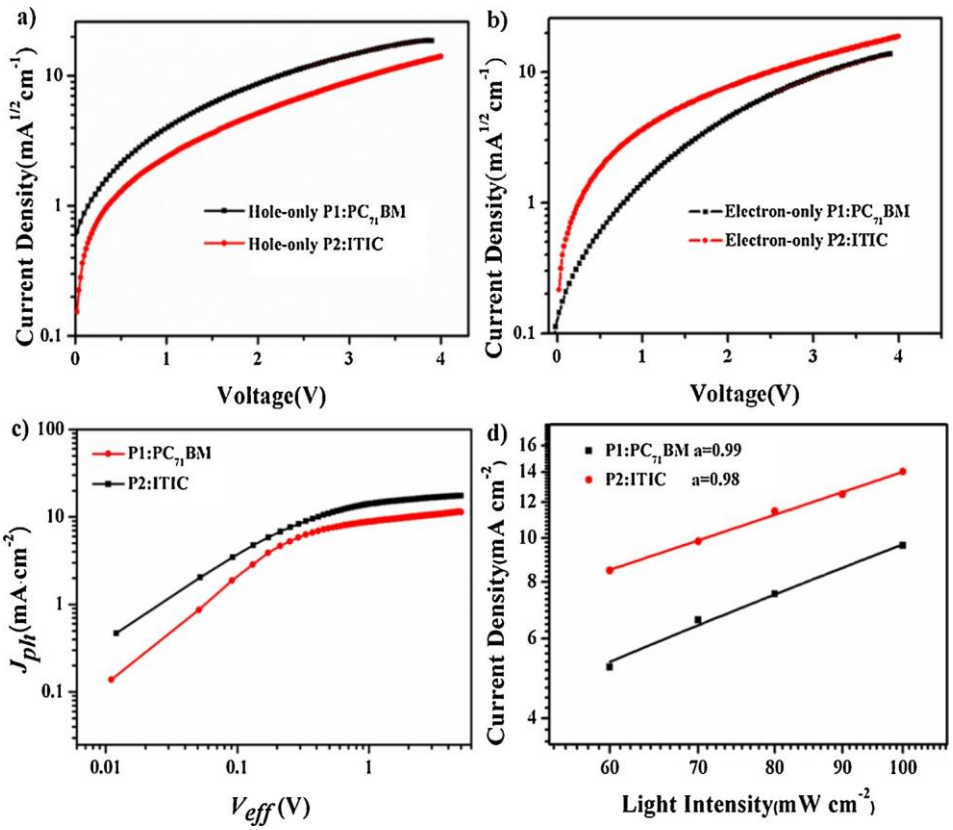

Fig. 6. (a) *J–V* characteristics of the hole-only devices and (b) electron-only devices fitted by the space-charge-limited current (SCLC) model; (c) photocurrent density (J_{ph}) and effective voltage (V_{eff}) curves of devices in the optimal conditions; (d) J_{sc} versus light intensity plots for optimized devices (The solid lines fitted the corresponding plots).

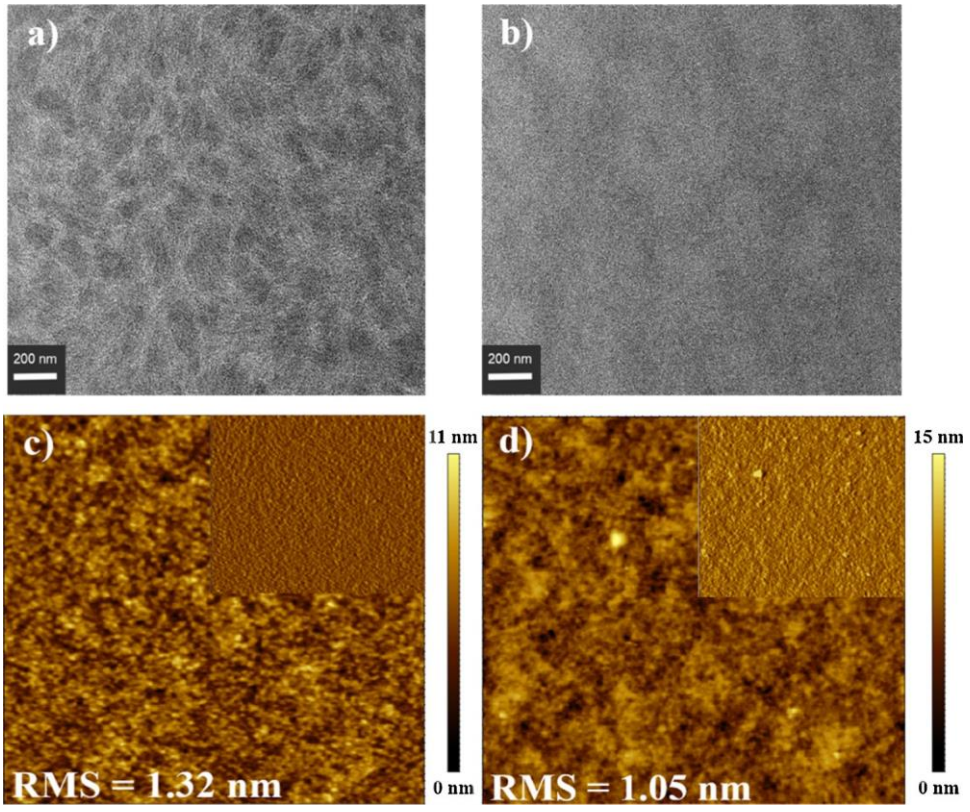

Fig. 7. TEM images and AFM images (5 μm x 5 μm) of (a) (c) P1: $PC_{71}BM$ blend; (b) (d) P2: ITIC blend in the optimized condition (the corresponding phase image are also given in c and d).

To study the charge transport behavior of electrons and holes in optimized devices based on synthesized polymers, the space-charge limited current (SCLC) method was used to obtain hole and electron mobility, with device structure of ITO/PEDOT:PSS/active layer (P1:$PC_{71}BM$ or P2:ITIC)/MoO_3/Al and ITO/ZnO/active layer (P1:$PC_{71}BM$ or P2:ITIC) /PDINO/Al. As shown in Fig. 6a and b, the hole mobility (μ_h) of P1:$PC_{71}BM$ and P2:ITIC blends are deduced as 1.03×10^{-4} and 0.76×10^{-4} cm^2 V^{-1} s^{-1}, while the electron mobility (μ_e) are 0.89×10^{-4} and 1.09×10^{-4} cm^2 V^{-1} s^{-1}respectively. The P1:$PC_{71}BM$ and P2:ITIC blends show balanced μ_e/μ_h ratio of 0.86 and 1.43, respectively, which is beneficial to charge transport.

To explore exciton separation and charge collection behavior of the devices based on P1 and P2, the exciton dissociation efficiencies (P_{diss}) are calculated from the relationship between photocurrent density (J_{ph}) and effective voltage (V_{eff}) [48]. The value of J_{ph} is calculated according to the follow formula: $J_{ph} = J_L$-J_D, where J_D and J_L represent light and dark current densities, respectively. The V_{eff} represents the difference value between the applied voltage (V_a) and the voltage V_0 (when J_{ph} is 0). As shown in Fig. 6c, the J_{ph} values of P1-based and P2-based PSCs are close to saturation and tend to stabilized value (J_{sat}) when the $V_{eff} > 1$, which reveals the values of P_{diss} reached maximum (P_{diss} is defined as J_{ph}/J_{sat}). The devices based on synthesized polymers in the optical conditions show similar P_{diss} of approximately 80%, indicating that the processes of photo-generated exciton dissociation and the free charge carries collection at the electrodes in the devices are efficient. Furthermore, as shown in Fig. 6d, the dependence of the photovoltaic performance on incident light power (ILP) was measured to study bimolecular recombination behavior in the optimized devices. The relationship between J_{sc} and light intensity is defined follow the equation of $J_{sc} \propto ILP^a$, where a is a power-law scaling exponent [49]. When the bimolecular recombination is weak, a value of the fitted line is approach to 1. The a value of devices based on P1 and P2 are 0.99 and 0.98 respectively, which reveals that the processes of bimolecular recombination are efficiently suppressed in the devices.

3.5. BHJ morphology properties

The transmission electron microscopy (TEM) and atomic force microscope (AFM) measurements were applied to further investigate the morphology characteristics of optimal blend films. As shown in Fig. 7a, we can observe continuous interpenetrating network structure in P1: $PC_{71}BM$ blend film. However, the obvious phase separation and polymer aggregation also occur, which will be bad for exciton diffusion to donor/acceptor interface and charge transport, and this lead to the low FF of devices. Contrast to P1:$PC_{71}BM$ blend, as shown in Fig. 7b, P2: ITIC blend exhibits good miscibility and less conspicuous polymer aggregation region. As a result, the J_{sc} of P2-based PSCs is higher than that of P1-based PSCs [50]. From Fig. 7c and d, the surface root mean square (RMS) roughness of both blends are small, which are helpful to form better contact with the electrodes [36].

4. Conclusions

In this work, D-A conjugated polymers P1 and P2 were designed and synthesized based on a novel monomer BBFBDT. The optical properties, electrochemical properties, photovoltaic properties, molecular conformations of polymers and the performance of BHJ PSCs based on synthesized polymers were investigated. When blended with acceptor $PC_{71}BM$, the device based on P1 exhibited the power conversion efficiency of 4.66% with V_{oc} of 0.93 V, J_{sc} of 9.83 mA cm^{-2} and FF of 50.97%. Contrast to P1, the wide band-gap polymer P2 shown relatively high power conversion efficiency of 6.59% with V_{oc} of 0.99 V, J_{sc} of 14.37 mA cm^{-2} and FF of 46.32% as a result of complementary absorption, suitable energy levels and aggregation, high EQE response and exciton dissociation (P_{diss}) when matched with non-fullerene acceptor ITIC. This work provides a reference for the design of polymer donor materials in the future.

Acknowledgements

The authors are deeply grateful to Fundamental Research Funds for the Central Universities (201822002) and Natural Science Foundation of Shandong Province (ZR2018MEM023), and National Natural Science Foundation of China (U1806223).

Appendix A. Supplementary data

Supplementary material related to this article can be found, in the online version, at doi:https://doi.org/10.1016/j.synthmet.2019.116182.

References

[1] L.-M. Chen, Z. Hong, G. Li, Y. Yang, Recent progress in polymer solar cells: manipulation of polymer: fullerene morphology and the formation of efficient inverted polymer solar cells, Adv. Mater. 21 (2009) 1434–1449.
[2] M.C. Scharber, N.S. Sariciftci, Efficiency of bulk-heterojunction organic solar cells, Prog. Polym. Sci. 38 (2013) 1929–1940.
[3] S. Li, L. Ye, W. Zhao, H. Yan, B. Yang, D. Liu, W. Li, H. Ade, J. Hou, A wide band gap polymer with a deep highest occupied molecular orbital level enables 14.2% efficiency in polymer solar cells, J. Am. Chem. Soc. 140 (2018) 7159–7167.
[4] Y. Li, Molecular design of photovoltaic materials for polymer solar cells: toward suitable electronic energy levels and broad absorption, Acc. Chem. Res. 45 (2012) 723–733.
[5] H. Li, Z. Xiao, L. Ding, J. Wang, Thermostable single-junction organic solar cells with a power conversion efficiency of 14.62%, Sci. Bull. 63 (2018) 340–342.
[6] Y. Zhou, W. Chen, Z. Du, D. Zhu, D. Ouyang, L. Han, R. Yang, High open-circuit voltage solution-processed organic solar cells based on a star-shaped small molecule end-capped with a new rhodanine derivative, Sci. China Chem. 58 (2015) 357–363.
[7] M. Zhang, X. Guo, W. Ma, S. Zhang, L. Huo, H. Ade, J. Hou, An easy and effective method to modulate molecular energy level of the polymer based on benzodithiophene for the application in polymer solar cells, Adv. Mater. 26 (2014) 2089–2095.
[8] J. Zhang, L. Zhu, Z. Wei, Toward over 15% power conversion efficiency for organic solar cells: current status and perspectives, Small Methods 1 (2017) 1700258.
[9] B. Fan, C. Sun, X.-F. Jiang, G. Zhang, Z. Chen, L. Ying, F. Huang, Y. Cao, Improved morphology and efficiency of polymer solar cells by processing donor-acceptor copolymer additives, Adv. Funct. Mater. 26 (2016) 6479–6488.
[10] G. Yu, C. Zhang, A.J. Heeger, Dual-function semiconducting polymer devices: light-emitting and photodetecting diodes, Appl. Phys. Lett. 64 (1994) 1540–1542.
[11] M. Zhang, Y. Gu, X. Guo, F. Liu, S. Zhang, L. Huo, T.P. Russell, J. Hou, Efficient polymer solar cells based on benzothiadiazole and alkylphenyl substituted benzodithiophene with a power conversion efficiency over 8%, Adv. Mater. 25 (2013) 4944–4949.
[12] J. Peet, J.Y. Kim, N.E. Coates, W.L. Ma, D. Moses, A.J. Heeger, G.C. Bazan, Efficiency enhancement in low-bandgap polymer solar cells by processing with alkane dithiols, Nat. Mater. 6 (2007) 497–500.
[13] Y. Liang, Z. Xu, J. Xia, S.T. Tsai, Y. Wu, G. Li, C. Ray, L. Yu, For the bright future-bulk heterojunction polymer solar cells with power conversion efficiency of 7.4%, Adv. Mater. 22 (2010) E135–E138.
[14] Q. Wan, X. Guo, Z. Wang, W. Li, B. Guo, W. Ma, M. Zhang, Y. Li, 10.8% efficiency polymer solar cells based on PTB7-Th and $PC_{71}BM$ via binary solvent additives treatment, Adv. Funct. Mater. 26 (2016) 6635–6640.
[15] Y. Lin, J. Wang, Z.G. Zhang, H. Bai, Y. Li, D. Zhu, X. Zhan, An electron acceptor challenging fullerenes for efficient polymer solar cells, Adv. Mater. 27 (2015) 1170–1174.
[16] Y. Xu, H. Yao, J. Hou, Recent advances in fullerene-free polymer solar cells: materials and devices, Chin. J. Chem. 37 (2019) 207–215.
[17] K. Dou, X. Wang, Z. Du, H. Jiang, F. Li, M. Sun, R. Yang, Synergistic effect of side-chain and backbone engineering in thieno[2,3-f]benzofuran-based conjugated polymers for high performance non-fullerene organic solar cells, J. Mater. Chem. A. 7 (2019) 958–964.
[18] W. Zhao, D. Qian, S. Zhang, S. Li, O. Inganäs, F. Gao, J. Hou, Fullerene-free polymer solar cells with over 11% efficiency and excellent thermal stability, Adv. Mater. 28 (2016) 4734–4739.
[19] Y. Firdaus, L.P. Maffei, F. Cruciani, M.A. Müller, S. Liu, S. Lopatin, N. Wehbe, G.O.N. Ndjawa, A. Amassian, F. Laquai, P.M. Beaujuge, Polymer main-chain substitution effects on the efficiency of nonfullerene BHJ solar cells, Adv. Energy Mater. 7 (2017) 1700834.
[20] S. Zhang, Y. Qin, J. Zhu, J. Hou, Over 14% efficiency in polymer solar cells enabled by a chlorinated polymer donor, Adv. Mater. 30 (2018) 1800868.
[21] J. Yuan, Y. Zhang, L. Zhou, G. Zhang, H.-L. Yip, T.-K. Lau, X. Lu, C. Zhu, H. Peng, P.A. Johnson, M. Leclerc, Y. Cao, J. Ulanski, Y. Li, Y. Zou, Single-junction organic solar cell with over 15% efficiency using fused-ring acceptor with electron-deficient core, Joule. 3 (2019) 1140–1151.
[22] H. Yao, L. Ye, H. Zhang, S. Li, S. Zhang, J. Hou, Molecular design of benzodithiophene-based organic photovoltaic materials, Chem. Rev. 116 (2016) 7397–7457.

[23] Y. Qin, L. Ye, S. Zhang, J. Zhu, B. Yang, H. Ade, J. Hou, A polymer design strategy toward green solvent processed efficient non-fullerene polymer solar cells, J. Mater. Chem. A 6 (2018) 4324–4330.
[24] J. Min, Z.-G. Zhang, S. Zhang, Y. Li, Conjugated side-chain-isolated D–A copolymers based on benzo[1,2-b:4,5-b′]dithiophene-alt-dithienylbenzotriazole: synthesis and photovoltaic properties, Chem. Mater. 24 (2012) 3247–3254.
[25] D. Lee, E. Hubijar, G.J.D. Kalaw, J.P. Ferraris, Enhanced and tunable open-circuit voltage using dialkylthio benzo[1,2-b:4,5-b′]dithiophene in polymer solar cells, Chem. Mater. 24 (2012) 2534–2540.
[26] J. Shin, M. Kim, J. Lee, D. Sin, H.G. Kim, H. Hwang, K. Cho, Effects of conformational symmetry in conjugated side chains on intermolecular packing of conjugated polymers and photovoltaic properties, RSC Adv. 5 (2015) 106044–106052.
[27] T. Zhu, D. Liu, K. Zhang, Y. Li, Z. Liu, X. Gao, X. Bao, M. Sun, R. Yang, Rational design of asymmetric benzodithiophene based photovoltaic polymers for efficient solar cells, J. Mater. Chem. A 6 (2018) 948–956.
[28] J.-H. Kim, J.B. Park, S.C. Yoon, I.H. Jung, D.-H. Hwang, Enhanced and controllable open-circuit voltage using 2D-conjugated benzodithiophene (BDT) homopolymers by alkylthio substitution, J. Mater. Chem. C 4 (2016) 2170–2177.
[29] C. Gao, L. Wang, X. Li, H. Wang, Rational design on D–A conjugated P(BDT–DTBT) polymers for polymer solar cells, Polym. Chem. 5 (2014) 5200–5210.
[30] F. Li, X. Song, K. Zhang, B. Shahid, Q. Wang, L. Yu, D. Zhu, M. Sun, Carbazole side-chained benzodithiophene based two-dimensional D-A conjugated photovoltaic polymers, Dye. Pigment. 170 (2019) 107548.
[31] X. Song, Y. Zhang, Y. Li, F. Li, X. Bao, D. Ding, M. Sun, R. Yang, Fluorene side-chained benzodithiophene polymers for low energy loss solar cells, Macromolecules 50 (2017) 6880–6887.
[32] Z. Cong, H. Liu, W. Wang, J. Liu, B. Zhao, Z. Guo, C. Gao, Z. An, Alternating polymers based on fluorinated alkoxyphenyl-substituted benzo[1,2-b:4,5-b′]dithiophene and isoindigo derivatives for polymer solar cells, Dye. Pigment. 146 (2017) 529–536.
[33] J. Shin, M. Kim, J. Lee, H.G. Kim, H. Hwang, K. Cho, Positional effects of fluorination in conjugated side chains on photovoltaic properties of donor-acceptor copolymers, Chem. Commun. 53 (2017) 1176–1179.
[34] J. Yuan, Y. Zou, R. Cui, Y.-H. Chao, Z. Wang, M. Ma, Y. He, Y. Li, A. Rindgen, W. Ma, D. Xiao, Z. Bo, X. Xu, L. Li, C.-S. Hsu, Incorporation of fluorine onto different positions of phenyl substituted benzo[1,2-b:4,5-b′]dithiophene unit: influence on photovoltaic Properties, Macromolecules. 48 (2015) 4347–4356.
[35] N. Wang, W. Chen, W. Shen, L. Duan, M. Qiu, J. Wang, C. Yang, Z. Du, R. Yang, Novel donor–acceptor polymers containing o-fluoro-p-alkoxyphenyl-substituted benzo[1,2-b:4,5-b′]dithiophene units for polymer solar cells with power conversion efficiency exceeding 9%, J. Mater. Chem. A 4 (2016) 10212–10222.
[36] D. Ding, J. Wang, W. Chen, M. Qiu, J. Ren, H. Zheng, D. Liu, M. Sun, R. Yang, Novel wide band gap polymers based on dithienobenzoxadiazole for polymer solar cells with high open circuit voltages over 1 V, RSC Adv. 6 (2016) 51419–51425.
[37] J. Wang, M. Xiao, W. Chen, M. Qiu, Z. Du, W. Zhu, S. Wen, N. Wang, R. Yang, Extending π-conjugation system with benzene: an effective method to improve the properties of benzodithiophene-based polymer for highly efficient organic solar cells, Macromolecules 47 (2014) 7823–7830.
[38] D. Qian, L. Ye, M. Zhang, Y. Liang, L. Li, Y. Huang, X. Guo, S. Zhang, Z. Tan, J. Hou, Design, application, and morphology study of a new photovoltaic polymer with strong aggregation in solution state, Macromolecules 45 (2012) 9611–9617.
[39] Y. Ie, J. Huang, Y. Uetani, M. Karakawa, Y. Aso, Synthesis, properties, and photovoltaic performances of donor–acceptor copolymers having dioxocycloalkene-annelated thiophenes as acceptor monomer units, Macromolecules 45 (2012) 4564–4571.
[40] H. Bin, Z.G. Zhang, L. Gao, S. Chen, L. Zhong, L. Xue, C. Yang, Y. Li, Non-fullerene polymer solar cells based on alkylthio and fluorine substituted 2D-conjugated polymers reach 9.5% efficiency, J. Am. Chem. Soc. 138 (2016) 4657–4664.
[41] F. Qi, J. Song, W. Xiong, L. Huo, X. Sun, Y. Sun, Two wide-bandgap fluorine-substituted benzotriazole based terpolymers for efficient polymer solar cells, Dye. Pigment. 155 (2018) 126–134.
[42] Y.-J. Cheng, J.-S. Wu, P.-I. Shih, C.-Y. Chang, P.-C. Jwo, W.-S. Kao, C.-S. Hsu, Carbazole-based ladder-type heptacylic arene with aliphatic side chains leading to enhanced efficiency of organic photovoltaics, Chem. Mater. 23 (2011) 2361–2369.
[43] Y. Zhong, D. Liu, K. Zhang, Y. Li, M. Sun, L. Yu, F. Li, H. Liu, R. Yang, Modifying the morphology via employing rigid phenyl side chains achieves efficient nonfullerene polymer solar cells, J. Polym. Sci. A Polym. Chem. 56 (2018) 2762–2770.
[44] Y. Li, G. Zhang, Z. Liu, X. Chen, J. Wang, C. Di, D. Zhang, Alternating Electron donor–acceptor conjugated polymers based on modified naphthalene diimide framework: the large enhancement of p-type semiconducting performance upon solvent vapor annealing, Macromolecules 46 (2013) 5504–5511.
[45] Z. Liu, D. Liu, K. Zhang, T. Zhu, Y. Zhong, F. Li, Y. Li, M. Sun, R. Yang, Efficient fullerene-free solar cells with wide optical band gap polymers based on fluorinated benzotriazole and asymmetric benzodithiophene, J. Mater. Chem. A 5 (2017) 21650–21657.
[46] Z. Li, H. Lin, K. Jiang, J. Carpenter, Y. Li, Y. Liu, H. Hu, J. Zhao, W. Ma, H. Ade, H. Yan, Dramatic performance enhancement for large bandgap thick-film polymer solar cells introduced by a difluorinated donor unit, Nano Energy 15 (2015) 607–615.
[47] Z. Liu, D. Liu, W. Chen, J. Wang, F. Li, D. Wang, Y. Li, M. Sun, R. Yang, Asymmetric 2D benzodithiophene and quinoxaline copolymer for photovoltaic applications, J. Mater. Chem. C 5 (2017) 6798–6804.
[48] Z. Liang, J. Tong, H. Li, Y. Wang, N. Wang, J. Li, C. Yang, Y. Xia, The comprehensive utilization of the synergistic effect of fullerene and non-fullerene acceptors to achieve highly efficient polymer solar cells, J. Mater. Chem. A 7 (2019) 15841–15850.
[49] P. Schilinsky, C. Waldauf, C.J. Brabec, Recombination and loss analysis in polythiophene based bulk heterojunction photodetectors, Appl. Phys. Lett. 81 (2002) 3885–3887.
[50] G.E. Park, S. Choi, S.Y. Park, D.H. Lee, M.J. Cho, D.H. Choi, Eco-friendly solvent-processed fullerene-free polymer solar cells with over 9.7% efficiency and long-term performance stability, Adv. Energy Mater. 7 (2017) 1700566.